Inhibition of Ricin A-Chain with Pyrrolidine Mimics of the Oxacarbenium Ion Transition State†

Setu Roday,‡ Timothy Amukele,‡ Gary B. Evans,§ Peter C. Tyler,§ Richard H. Furneaux,§ and Vern L. Schramm*,‡

Department of Biochemistry, Albert Einstein College of Medicine, 1300 Morris Park Avenue, Bronx, New York 10461, and Carbohydrate Chemistry Team, Industrial Research Ltd., Lower Hutt, New Zealand

Received January 20, 2004; Revised Manuscript Received February 26, 2004

ABSTRACT: Ricin A-chain (RTA) catalyzes the hydrolytic depurination of a specific adenosine at position 4324 of 28S rRNA. Kinetic isotope effects on the hydrolysis of a small 10mer stem−tetraloop oligonucleotide substrate established the mechanism of the reaction as D_N*A_N, involving an oxacarbenium ion intermediate in a highly dissociative transition state. An inhibitor with a protonated 1,4-dideoxy-1,4-imino-D-ribitol moiety, a 4-azasugar mimic, at the depurination site in the tetraloop of a 14mer oligonucleotide with a 5 bp duplex stem structure had previously been shown to bind to RTA with a K_d of 480 nM, which improved to 12 nM upon addition of adenine. Second-generation stem−tetraloop inhibitors have been synthesized that incorporate a methylene bridge between the nitrogen of a 1-azasugar mimic, namely, (3*S*,4*R*)-3-hydroxy-4-(hydroxymethyl)pyrrolidine, and substituents, including phenyl, 8-aza-9-deazaadenyl, and 9-deazaadenyl groups, that mimic the activated leaving group at the transition state. The values for the dissociation constants (K_i) for these were 99 nM for the phenyl 10mer, 163 and 94 nM for the 8-aza-9-deazaadenyl 10- and 14mers, respectively, and 280 nM for the 9-deazaadenyl 14mer. All of these compounds are among the tightest binding molecules known for RTA. A related phenyl-substituted inhibitor with a deoxyguanosine on the 5′-side of the depurination site was also synthesized on the basis of stem−loop substrate specificity studies. This molecule binds with a K_i of 26 nM and is the tightest binding "one-piece" inhibitor. 8-Aza-9-deaza- and 9-deazaadenyl substituents provide an increased pK_a at N7, a protonation site en route to the transition state. The binding of these inhibitors is not improved relative to the binding of their phenyl counterpart, however, suggesting that RTA might also employ protonation at N1 and N3 of the adenine moiety to activate the substrate during catalysis. Studies with methylated adenines support this argument. That the various stem−loop inhibitors have similar potencies suggests that an optimal one-piece inhibitor remains to be identified. The second-generation inhibitors described here incorporate ribose mimics missing the 2-hydroxy group. On the basis of inhibition data and substrate specificity studies, the 2′-hydroxyl group at the depurination site seems to be critical for recruitment as well as catalysis by RTA.

Ricin is an extremely cytotoxic protein from castor beans that inhibits protein synthesis in cells by depurination of ribosomes at a site where elongation factors bind during translation. The B-chain of this heterodimeric protein is a lectin that serves to direct the catalytic A-chain to the cell surface. Within the cytosol, ricin toxin A-chain (RTA)[1] binds to a specific "GAGA" nucleotide sequence on the sarcin−ricin loop (SRL) of the 28S ribosomal RNA and specifically depurinates the first adenosine (A_{4324} on the ribosome) in that sequence (*1*) (Figure 1). Previous work in this laboratory (*2*) established the mechanism of depurination as D_N*A_N (*3*), involving an oxacarbenium ion intermediate and a highly dissociative transition state. This work was based on interpretations of the kinetic isotope effects on the hydrolysis of a small 10mer stem−tetraloop oligonucleotide substrate, A-10 (Figure 2).

This isotope effect study laid the foundation for the design of short stem−tetraloop inhibitors incorporating structural features of the oxacarbenium ion-like transition state at the depurination site. One such inhibitor, 1N-14 (Figure 2), which featured a (3*S*,4*R*)-3-hydroxy-4-(hydroxymethyl)-pyrrolidine at the depurination site in the tetraloop of a 14mer oligonucleotide with a 5 bp duplex stem structure, was shown to bind to RTA with a K_d of 0.48 μM, which improved to 12 nM upon addition of adenine (*4*). This result was consistent with the unusual dissociative mechanism.

Most of our recent work on inhibitor design has sought to address some of the questions posed by the tight binding of a ternary complex of the stem−loop inhibitor, 1N-14 with RTA and adenine. The binding of the binary complexes, IR-10 and 1N-14 (Figure 2) with RTA are comparable (K_d = 1.3 and 0.48 μM, respectively), but the affinity of 1N-14

† This work was supported by NIH Grant CA7244.

* To whom correspondence should be addressed. Telephone: (718) 430-2777. Fax: (718) 430-8565. E-mail: vern@aecom.yu.edu.

‡ Albert Einstein College of Medicine.

§ Industrial Research Ltd.

[1] Abbreviations: RTA, ricin toxin A-chain; SRL, sarcin−ricin loop; A-10, 5′-CGC GAGA GCG-3′; TS, transition state; DADMe-A, 1-[(9-deazaaden-9-yl)methyl]-(3*S*,4*R*)-3-hydroxy-4-(hydroxymethyl)pyrrolidine; DMT, dimethoxytrityl; DMAP, 4-(dimethylamino)pyridine; TLC, thin-layer chromatography; EDTA, ethylenediaminetetraacetic acid; HMBC, heteronuclear multiple-bond correlation spectroscopy; FMP, formycin monophosphate.

10.1021/bi0498499 CCC: $27.50
Published on Web 04/09/2004

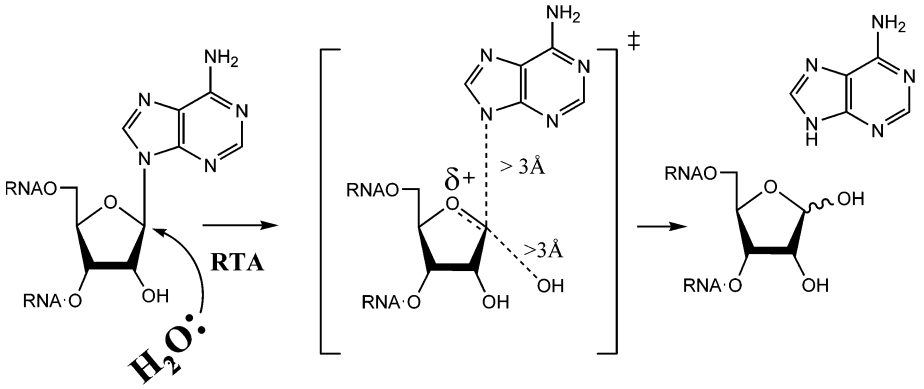

FIGURE 1: Hydrolytic cleavage of an adenosine moiety catalyzed by RTA that proceeds through an "oxacarbenium" ion transition state.

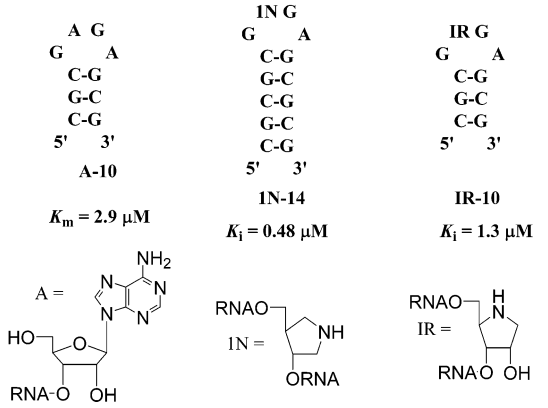

FIGURE 2: Stem−tetraloop substrate, A-10, and the pyrrolidine-containing inhibitors, IR-10 and 1N-14. Moving the nitrogen atom in the pyrrolidine nucleus from the equivalent of the 4′-position of ribose to the 1′-position results in a 2-fold improvement in affinity.

is enhanced almost 2 orders of magnitude in the ternary complex (K_d = 12 nM). The binding in pieces of 1N-14 and adenine represents a reorganization of components in the active site that may resemble the transition state of the RTA catalytic reaction.

The design of new stem−loop structures is aimed at finding a tight binding one-piece inhibitor of RTA. Covalent linkage was included in the design to compensate for the loss of binding energy from the entropic cost associated with the reorganization of pieces. The gain in binding strength (of as much as 5−9 kcal/mol) when fragments are connected together results from a loss of translational and rotational entropy in a tight transition state (*5*).

The covalent design strategy incorporates a methylene bridge between the nitrogen and the adenine ring to provide sufficient torsional flexibility for an adaptive placement of the ring in the active site. The pyrrolidine nitrogen ($pK_a \sim 8.5$) (*6*) is protonated under the assay conditions and thus mimics the positive charge on C1′ of a delocalized oxacarbenium ion in the transition state. On the basis of these hypotheses, various inhibitors were conceived with adenine and structurally analogous rings linked by a methylene bridge to the pyrrolidine nitrogen at the depurination site (Figure 3). This paper describes the syntheses and characterization of these inhibitors.

RTA has been used in designing immunotoxin constructs by linking it to an antibody that can target cancer cells carrying specific antigenic markers (*7*). Such approaches show promise but are compromised by specificity issues.

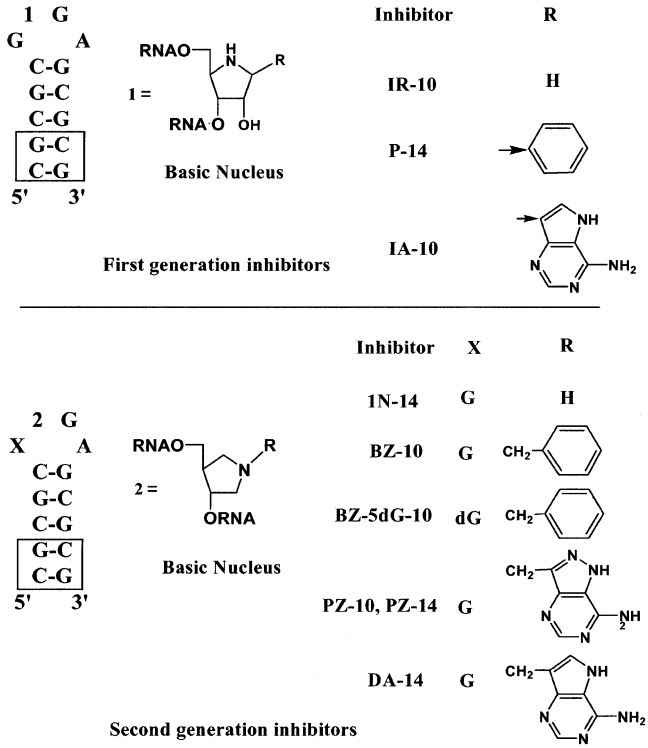

FIGURE 3: First- and second-generation pyrrolidine-containing inhibitors that resemble the oxacarbenium ion transition state of the RTA reaction. All first-generation compounds and second-generation compound 1N-14 have been discussed in refs *4* and *12*, respectively. All other second-generation compounds were synthesized and characterized as a part of this work.

Tight binding transition state inhibitors may provide a novel way of rescuing patients from the toxicity associated with such therapies.

MATERIALS AND METHODS

Materials and General Experimental. RTA was purchased from Sigma. Calf intestinal alkaline phosphatase was from Promega (Madison, WI), and phosphodiesterase I was from Sigma Chemical Co. (St. Louis, MO). RNase inhibitors and RNase-free DNase were from Ambion (Austin, TX). Nucleoside phosphoramidites and other reagents for oligoribonucleotide synthesis were purchased from Glen Research (Sterling, VA), except for phosphoramidites attached directly to CPG solid supports, which were obtained from ChemGene Corp. (Ashland, MA). [8-^{13}C;6,9-^{15}N]Adenine was purchased from Cambridge Isotopes. The adenine analogue 9-deazaadenine was synthesized by Industrial Research Ltd. All other

Scheme 1 [a]

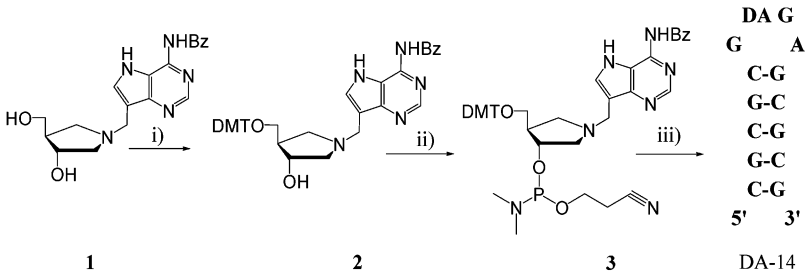

[a] (i) DMTrCl (1.5 equiv), DMAP (catalytic), (*i*Pr)$_2$NEt (2 equiv), pyridine, room temperature, 5 h; (ii) 2-cyanoethyl *N*,*N*-diisopropylchlorophosphoramidite (2.5 equiv), 2,4,6-collidine (2.5 equiv), 1-methylimidazole (1 equiv), methylene chloride, 0 °C, 30 min; (iii) Expedite DNA/RNA synthesis system.

chemicals were purchased from Aldrich Chemical Co. (Milwaukee, WI) and were of the highest purity available. These reagents were used without further purification. Purification of reaction intermediates of the phosphoramidite synthetic pathway was completed by flash column chromatography using Merck silica gel 60 (230−400 mesh). Purification by HPLC was performed on a Waters 626 pump with a 996 photodiode array detector and using the Millennium software package. RNA concentrations were determined by UV−vis measurements using a Cary 100 diode array spectrophotometer from Varian.

Synthesis of the Nucleoside Phosphoramidite Analogues. For the synthesis of phosphoramidite 3, (3*R*,4*S*)-3-hydroxy-4-(hydroxymethyl)pyrrolidine was synthesized from D-xylose (*8*) and converted to the N^6-benzoyl derivative **1** by the Mannich reaction with formaldehyde and the requisite 9-deazapurine (*9*). As shown in Scheme 1, **1** was converted to the dimethoxytrityl (DMTr) ether **2**, purified by column chromatography, and reacted with phosphitylation reagent following a standard procedure. Briefly, to a solution of **2** (100 mg, 0.15 mmol) in dry methylene chloride (15.0 mL) at 0 °C under an argon atmosphere were added quickly 2,4,6-collidine (53 μL, 0.4 mmol), 2-cyanoethyl *N*,*N*-diisopropylchlorophosphoramidite (80 μL, 0.36 mmol) and 1-methylimidazole (10 μL, 0.11 mmol). The reaction mixture was then warmed to room temperature and stirred for 30 min to afford phosphoramidite **3**, the completion of the reaction being confirmed by TLC. This product was used directly in the synthesis of DA-14 without purification since it is very unstable. The other phosphoramidites were synthesized analogously.

Synthesis and Purification of Oligonucleotides. Oligo(ribo and deoxy)nucleotides were chemically synthesized using a phosphoramidite methodology on an Expedite 8900 Nucleic Acid Synthesis System from Perseptive Biosystems. Syntheses were carried out on a 1 μmol scale with coupling times extended to 15 min, in the trityl-off mode. The coupling times for guanosine and deoxyguanosine were extended to 40 min. Deprotection of the products was accomplished using a concentrated NH_4OH/ethanol mixture (3:1, v/v) (*10*) and triethylamine trihydrofluoride (*11*) as described by Chen *et al.* (*12*). All products were purified by HPLC using a Waters XTerra Prep MS C18 column (7.8 mm × 50 mm). These columns are specially designed for purification of oligonucleotides in the trityl-off mode and employ an ion pairing mobile phase of 50 mM triethylammonium carbonate (pH 6.4) with a gradient from 3 to 80% of 50% methanol. The homogeneity of each product was confirmed by ion exchange chromatography on a Protein-Pak Q-15 HR DEAE column eluted with 50 mM ammonium acetate (pH 5.0) containing 15% methanol and 1.0 M LiCl. The nucleotide composition was determined by enzymatic digestion of a 50 μL aliquot of a 2.5−5 μM solution of the oligonucleotide with 1 unit each of calf intestinal alkaline phosphatase and snake venom phosphodiesterase I overnight at 37 °C, and quantitation of the released nucleosides relative to known standards by HPLC on a Waters Delta-Pak C18 analytical column (3.9 mm × 300 mm) eluted with 50 mM ammonium acetate (pH 5.0) containing 5% methanol. Nucleoside and deoxynucleoside standards were used to determine the relative amounts of each component in the digest. Product formation for all stem−loop compounds was further confirmed by MALDI-TOF mass spectrometry analysis on an Applied Biosystems 4115 Voyager system. Masses were acquired in the 500−5000 Da range.

Inhibition Kinetics. Reaction rates were determined in 10 mM potassium citrate buffer (pH 4.0) containing 1 mM EDTA. The total reaction volume was 100 μL. Reactions were started by the addition of RTA at concentrations of 26−48 nM. After incubation of the reaction vials at 37 °C for the allotted time, the reactions were quenched by inactivating the enzyme with 50 mM potassium phosphate buffer (pH 8.3, 100 μL of a 1 M solution). The samples were then injected onto a reversed-phase C18 Waters Delta-Pak guard and analytical column (3.9 mm × 300 mm) with isocratic elution in 50 mM ammonium acetate (pH 5.0) containing 5% methanol, at a flow rate of 1 mL/min. The enzyme protein is retained on the guard column under these conditions. The extent of hydrolysis of RNA by RTA was measured by quantitating the released adenine by monitoring the peak at 260 nm and using a comparison with standards treated with the same protocol. Both the substrate and inhibitors were heated to 80 °C for 1 min, cooled on ice, and incubated at 37 °C for 15 min prior to their addition to the assay mix to reduce the variability in the turnover rate that can result from conformational heterogeneity (hairpins vs other forms) in solution. In initial rate experiments, the extent of substrate hydrolysis was less than 15%. Product formation was shown to conform to initial rate conditions for the duration of the assay. Values for the inhibition dissociation constant (K_i) were determined by fitting the initial rates to the equation for competitive inhibition, $v = k_{cat}[S]/[[S] + K_m(1 + I/K_i)]$, where v is the initial reaction rate, [S] is the substrate concentration, K_m is the Michaelis constant (2.9 μM for the competitive substrate, A-10, under the assay conditions), I is the inhibitor concentration, and

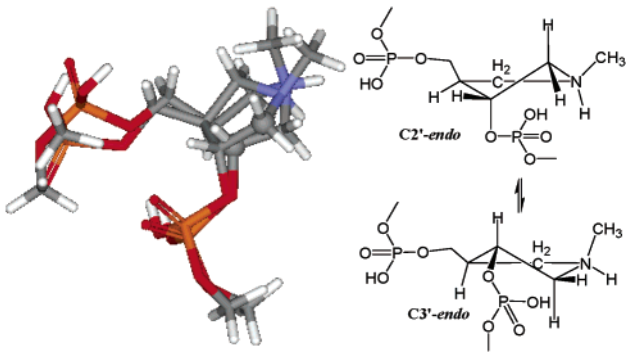

FIGURE 4: Superimposed 2′- and 3′-endo conformations of a model 1-azasugar in vacuo obtained from a Monte Carlo search using the Amber 99 force field implemented within the Hyperchem program. The 5′- and 3′-phosphate chains can adopt similar spatial orientations in both without a significant energetic cost.

k_{cat} is the rate of catalytic turnover at substrate saturation. The concentration range of 7−15 μM used for A-10 in this assay represents values that are 2.5−5 times above its K_m, and was a convenient range for competitive inhibitor analysis (*13*). The inhibitor concentration was kept at >5 times that of the enzyme except for one case of a strong inhibitor where enzyme and inhibitor concentrations were similar. The free inhibitor concentration was determined by the relationship $I = I_t - (1 - v_i/v_o)E_t$, where I_t is total inhibitor concentration, v_i and v_o are the inhibited and uninhibited steady state rates, respectively, and E_t is the total enzyme concentration. For rates involving a ternary complex, the substrate and inhibitor concentrations were kept constant and the purine concentration was varied. The K_i values for these compounds were determined using the thermodynamic cycle shown in Figure 5f. The data for activation and inhibition kinetics seen with DADMe-A were fitted to a two-site binding model using the equation $v = k_{cat}[S]/([S] + K_m) + k'_{cat}/(1 + K'_i/I + I/K_i)$, where [S] is the substrate concentration and K'_i is the binding constant of the inhibitor for the activation site. This assumes that the inhibitor binds to both the free enzyme and the enzyme−substrate complex (ES) and that the ESI complex is productive at a rate represented by k'_{cat} (*14*).

NMR Spectroscopic Determination of the pK_a of Adenine at N9. NMR experiments in D_2O were performed at 25 °C on a Bruker DRX 300 MHz spectrometer equipped with pulsed-field gradients. 3-(Trimethylsilyl)propionic-2,2,3,3-d_4 acid sodium salt was used as the internal standard to which the ^{1}H chemical shifts were referenced and ^{15}N resonances were indirectly referenced. To obtain the pK_a value of N9 of adenine, two-dimensional ^{1}H−^{15}N HMBC experiments were carried out for [8-^{13}C;6,9-^{15}N]adenine at several pH values. Sweep widths of 6083.6 Hz (^{15}N) and 4194.63 Hz (^{1}H) were used with the nitrogen and proton carriers set at 200 and 4.69 ppm, respectively. Titrations were performed by adding small aliquots of 0.1 M NaOH or HCl. The pK_a value for N9 of the adenine was determined by following the pH-dependent chemical shifts of the 8-proton and the 9-nitrogen. The titration data were fitted to the equation pK_a = $\delta_1 - (\delta_1 - \delta_2)/(1 + 10^{\delta - pH})$, where δ_1 and δ_2 are the limiting chemical shifts at low and high pH, respectively.

RESULTS AND DISCUSSION

Basis for the Design of Inhibitors that Feature Pyrrolidines (4-Azasugars) at the Depurination Site on a Stem−Tetraloop Oligonucleotide: The "First-Generation" Compounds. Specificity and isotope effect studies with RTA established that leaving group activation was the primary mechanism of depurination. The transition state of the reaction is highly dissociative (D_N*A_N) and proceeds through an oxacarbenium ion intermediate which forms without nucleophilic assistance so that there is virtually no bond order to the nucleophile and an insignificant residual bond order to the leaving group so that the C1′−N9 glycosidic bond length is greater than 3.0 Å. This imparts an increased cationic character to C1′ as a result of delocalization of electrons from the lone pairs of the ring oxygen toward the reaction center. The O−C1′ bond thus has partial double bond character, and the cationic C1′ has planar sp^2 character. Inhibitors described in previous work from this laboratory such as IA-10 (*4*) and P-14 (*12*) were stem−tetraloop analogues (Figure 3) that incorporated iminoribitol derivatives (X) as nonhydrolyzable isosteres for adenosine in the depurination site on the loop (i.e., GXGA in place of GAGA). These compounds were the first-generation pyrrolidines synthesized for inhibition of RTA. IA-10 has a nonhydrolyzable 1-(9-deazaadenin-9-yl)iminoribitol, Immucillin-A (IA), incorporated into a 10mer RNA stem−loop (Figure 3). The pyrrolidine ring nitrogen of this compound mimics the oxacarbenium ion of the ribosyl ring at the transition state of the RTA-catalyzed hydrolytic reaction. The pK_a of N7 in 9-deazaadenosine is greater than 12 (*15*), and this design feature ensured that the 9-deazaadenyl ring would resemble an activated leaving group at the transition state. A H-bond from N7 to an amino acid residue on the enzyme is consistent with the inverse isotope effect observed at N7 for the hydrolysis of A-10 by RTA (*3*). P-14 incorporated similar features except that a phenyl ring was substituted for 9-deazaadenine. Since 9-deazaadenine resembles the adenyl substituent at the TS more closely than the phenyl, it was surprising that P-14 bound approximately 2.5 times better than IA-10. However, the 6−12-fold gain in affinity of IA-10 and P-14 over the substrate A-10, respectively (Table 1), is smaller than that expected of a transition state analogue. Iminoribitols possess a covalent C−C bond between C1′ and the 9-deazapurine group which is ~1.5 Å long, but this is at least 1.5 Å shorter than the distance (3.0 Å) that separates the corresponding atoms at the transition state. Thus, the 9-deazaadenyl substituent in IA-10 and the phenyl ring in P-14 are geometrically constrained in their ability to mimic the reaction coordinate distance at the actual transition state.

It was therefore thought that placing the carbocation charge in the inhibitor closer to its location in the transition state and spacing the iminoribitol and the leaving group closer to the actual transition state distances may enhance affinity. This led to the synthesis of second-generation pyrrolidines as inhibitors of RTA. The endocyclic ring nitrogen in these structures is shifted to where C1′ would be in a ribose ring (such structures can also be designated as 1-azasugars). Among abasic inhibitors previously characterized in this laboratory, 1N-14 which possesses the 1-azasugar structure was bound 2-fold tighter than IR-10 which possesses an iminoribitol structure (*4*). The pK_a values of the ring nitrogens in both these structures are close to 6.5 (*12*, *16*), but the former is better able to mimic the actual transition state characteristics since protonation of the 1-azasugar nitrogen provides a direct mimic of the C1′ carbocation that exists at

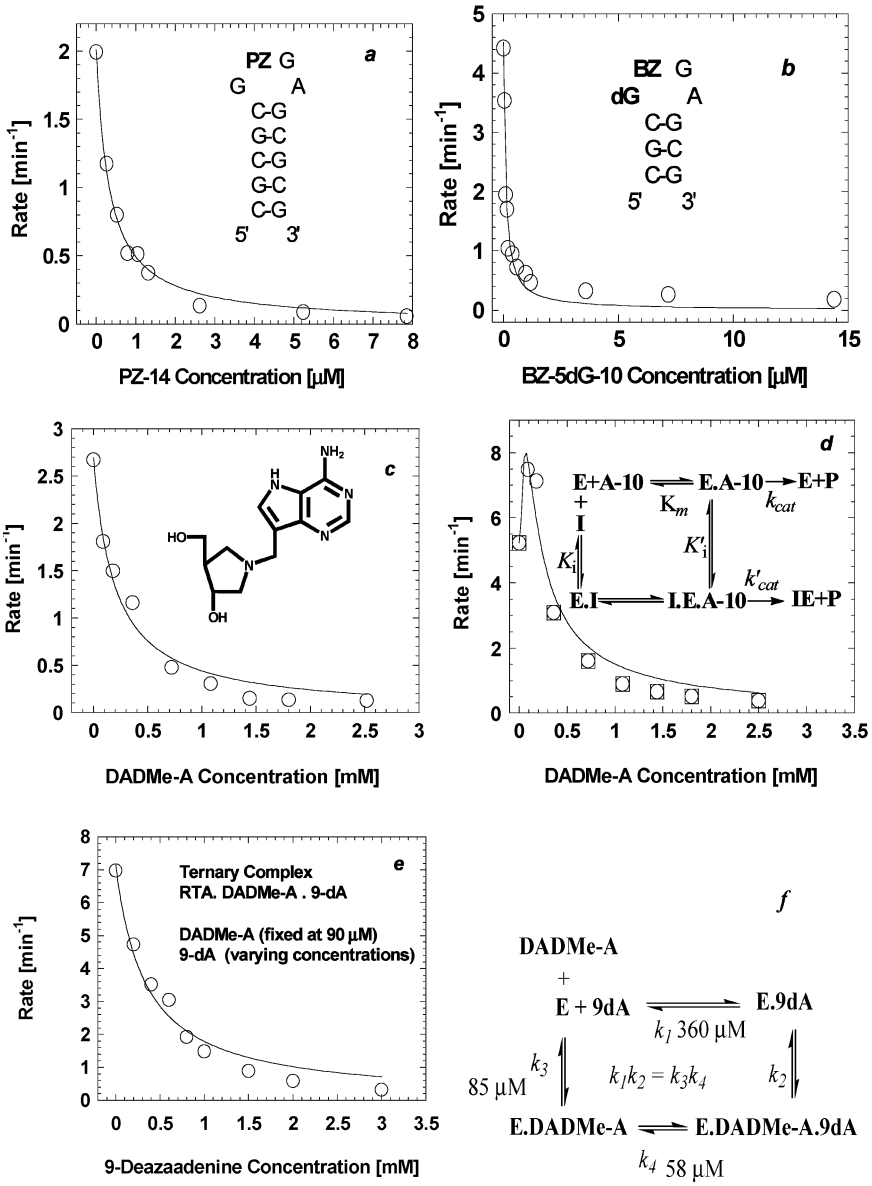

FIGURE 5: Plots for the determination of K_i values for competitive inhibitors. (a) Inhibition by PZ-14. The K_i was determined from fits of initial rate data vs inhibitor concentration to the equation $v = k_{cat}[S]/([S] + K_m(1 + I/K_i)]$. The inhibition constants for all other compounds described in this work were determined from similar fits to the equation. (b) Inhibition by BZ-5dG-10. The data were fitted to the equation for tight binding inhibitors in which the inhibitor concentration is within 1-fold of the enzyme concentration, $v = k_{cat}[S]/([S] + K_m\{1 + [I_t - (1 - v_i/v_o)E_t]/K_i\})$, where I_t is the total inhibitor concentration, v_i and v_o are inhibited and uninhibited steady state rates, respectively, and E_t is the total enzyme concentration. (c) Inhibition by DADMe-A at a substrate concentration of 3.5 μM in the competitive assay. (d) Activation by DADMe-A at a substrate concentration of 14 μM. The squares represent data that were fitted to the equation for competitive inhibition ignoring the activation phase. The circles represent data that were fitted to a two-site binding model using the equation $v = k_{cat}[S]/([[S] + K_m) + k'_{cat}/(1 + K'_i/I + I/K_i)]$, assuming that the inhibitor binds to both the free enzyme and the enzyme−substrate complex (ES) and that the ESI complex is productive at a rate represented by k'_{cat}. [S] is the substrate concentration, and K'_i is the binding constant of the inhibitor for the activation site. (e) Inhibition of a ternary complex of RTA, DADMe-A, and 9-deazaadenine. (f) Thermodynamic cycle for assessing binding of the ternary complex.

substrate transition states that are highly dissociative. It was further shown in the same work that the affinity of 1N-14 is enhanced almost 1 order of magnitude in a ternary complex with RTA and adenine (K_d = 12 nM). The binding in pieces of 1N-14 therefore represents a better capture of the transition state energy of the RTA catalytic reaction. It was therefore thought that introduction of a methylene bridge between the 1-azasugar nitrogen and the deazapurine would provide an additional 1 Å between these groups while retaining the favorable pK_a at N7 needed for the 2−3 kcal/mol gain in strength from an H-bond at the transition state. On the basis of Wolfenden's hypothesis, such a covalent assemblage of pieces could regain up to 4−5 kcal/mol of binding energy that is otherwise lost from the entropic cost of bringing components together in a noncovalent fashion (*5*). The nitrogen atom corresponding to C1′, with an attached methylene bridge, has a pK_a value near 8.5 (*6*) and would thus be fully protonated and retain its cationic nature at physiological pH and under the assay conditions at pH 4.0. The protonated tertiary nitrogen of the pyrrolidine would not only mimic the ionization state at C1′ but also be geometrically similar.

Inhibition of RTA with All-RNA Stem−Tetraloop Hairpins Incorporating Methylene-Bridged 1-Azasugars at the Depu-

Table 1: Kinetic Constants for the RTA-Catalyzed Reaction of Substrates A-10 and 5dG8dA-12 and Competitive Inhibition Constants for the Inhibitors[a]

inhibitor	K_i (μM)[b]	inhibitory potency relative to TC[d]
1N-14−RTA−Ade	0.012	1
A-10 (substrate)	2.9 (K_m)	241
P-14	0.18 ± 0.02	15
IA-10	0.57 ± 0.06	47
IR-10	1.3	108
1N-14	0.48	40
BZ-10	0.099 ± 0.013	8
PZ-10	0.163 ± 0.008	13
PZ-14	0.094 ± 0.007	7
DA-14	0.280 ± 0.004	23
BZ-5dG-10[c]	0.026 ± 0.003	2
PZ-4	22 ± 3	1833
PZ-6	43 ± 6	3583
DADMe-A	88 ± 12	7300
DADMe-A−RTA−9dA	21	1800
5dG8dA-12[e]	0.76 ± 0.11	∼66
(substrate)	0.86 ± 0.15	
1-methyladenine	600 (IC_{50})	50000
3-methyladenine	900 (IC_{50})	75000
9-methyladenine	*f*	−

[a] The first six rows give inhibitors that were characterized in previous work from this group and data taken from refs *4* and *12*. [b] K_i values were determined from fits of initial rate data vs inhibitor concentration to the equation $v = k_{cat}[S]/([S] + K_m(1 + I/K_i))$. [c] The data were fitted to the equation $v = k_{cat}[S]/([S] + K_m\{1 + [I_t - (1 - v_i/v_o)E_t]/K_i\})$. [d] TC is the RTA−1N-14−adenine ternary complex. All K_i values have been compared to that of the ternary complex. [e] 5dG8dA-12 was characterized against two competitive substrates, A-10 and 6dA-10. [f] Not determined.

rination Site: The "Second-Generation" Compounds. On the basis of these findings, the second-generation methylene-bridged 1-azasugars (BZ-10, PZ-10, PZ-14, and DA-14) were synthesized and tested as inhibitors of RTA in this work (Figure 3). BZ-10 was found to inhibit RTA with a K_i of 99 nM, which is ∼2-fold better than P-14 which had a K_i of 180 nM as described in Table 1. The gain in affinity is consistent with the ability of the pyrrolidine ring in BZ-10 to better mimic the carbenium ion and of the phenyl group to interact with the leaving group pocket on the enzyme. The interactions between RTA and several nucleotides and nucleotide analogues have been analyzed by X-ray crystallography (*17*). Tyr80 and Tyr123 are proposed to contribute to leaving group activation by π-stacking with adenine, while Glu177 is proposed to stabilize the proposed developing oxacarbenium ion charge on the ribosyl ring by an electrostatic interaction. Although there are no structural data, the enhanced binding of BZ-10 relative to P-14 may result from more favorable π-stacking of the phenyl ring between Tyr80 and Tyr123 since the methylene bridge in the former is able to provide torsional flexibility to the phenyl group, enabling the correct binding orientation. However, the mechanism of stabilization of the protonated pyrrolidine nitrogen under these conditions (pH 4.0) is unclear since Glu177 would be expected to be protonated.

The adenine heterocycle possesses three sites (N1, N3, and N7) at which potential electrostatic or H-bond interactions with the enzyme can assist the electron withdrawal needed to facilitate N-ribosidic bond loss. Electrostatic interactions are significant in the enzymes that employ leaving group activation, including excision repair DNA glycosylases. Subtle differences in the nature of these interactions can have remarkable consequences such as prevention of enzyme promiscuity in recognizing substrates (*18*−*20*). The inverse isotope effects observed at N7 of adenine during the RTA-catalyzed hydrolysis of A-10 suggested that this was a site of protonation en route to the transition state, but isotope effects at N1 and N3 have not yet been determined. Molecules PZ-10, PZ-14, and DA-14 contain heterocyclic isosteres for adenine and were designed to be similar to IA-10 (*4*) in an attempt to gain affinity over the phenyl compound.

PZ-10 and PZ-14 had K_i values of 163 and 94 nM, respectively, while DA-14 had a K_i value of 280 nM. DA-14 with a 9-deazaadenyl substituent most closely resembles adenine. The somewhat weak binding of this molecule was therefore surprising. The "PZ" compounds possess an 8-aza-9-deazaadenine moiety akin to that found in the C-glycoside, Formycin A, a transition state inhibitor of AMP nucleosidase. The Formycin A structure had previously been incorporated into a stem−loop analogue, F-10, which had a K_i of 9 μM (*12*). The PZ compounds bind ∼90-fold better than F-10, and this likely stems from the improved ability of the putatively cationic pyrrolidine ring of the former to mimic the transition state. The X-ray structure of formycin monophosphate (FMP) in complex with RTA shows that the base adopts a *syn* conformation and is packed snugly in a binding pocket surrounded by several side chain contacts (*17*, *21*). FMP was bound poorly though (K_i ∼ 1 mM), and the possibility that the 8-aza-9-deazaadenine group in F-10 may similarly adopt a *syn* conformation was suggested in an earlier paper to explain its poor activity (*12*). However, new data on restrictocin−inhibitor complexes indicate that ribosome-inactivating proteins such as ricin may use a base flipping mechanism to dock its target (GAGA) in the active site before depurination (*22*, *23*). For the stem−loop substrates to dock in a similar manner, base flipping of adenosine would have to occur, resulting in disruption of base stacking with the adjacent 3′-side guanosine. It is likely that the tetraloop unfolds on binding to RTA, and the energy required for this transformation could be as little as 1−2 kcal/mol (*24*). In the NMR solution structure of the sarcin−ricin loop (SRL) RNA (*25*, *26*), the glycosidic bond of the susceptible adenosine is *anti* and a base flipping on binding to RTA would dispose it in a *syn* orientation prior to catalysis. We would have predicted a favorable interaction for the 8-aza-9-deazaadenine moiety of F-10 on the basis of the possibility that the methylene bridge of PZ compounds would provide flexibility for the base to adopt a favorable orientation (either *syn* or *anti*). Although this may also explain the better binding of PZ-10 and PZ-14 over F-10, the lack of structural data makes it difficult to provide a clear explanation for the observations.

None of the three molecules with a methylene bridge to a heterocyclic base, however, provided any advantage in affinity over their phenyl counterpart, BZ-10. This suggests that the 8-aza-9-deazaadenine and 9-deazaadenine moieties do not provide any energetic advantage over the phenyl group despite the elevated pK_a (for both, greater than 9) at N7 required for the purported H-bond at the transition state. This inhibition study suggests it is likely that RTA-catalyzed hydrolysis of adenosine proceeds via protonation of adenine at multiple sites with contributions from N1 and N3 which may be more important than that from N7. X-ray crystal-

lographic studies suggest that Arg180 is responsible for full or partial protonation of N3 of adenine (*17*). Mutation of this residue reduces the k_{cat} by 500-fold (*27*); while the effect is substantial, it is clearly not essential. It is proposed then that under physiological conditions the role of Arg180 in protonation of the adenine moeity is diminished because it forms an ion pair with Glu177.

It is possible that RTA uses different mechanisms of substrate activation under physiological conditions than under the *in vitro* assay conditions that require a pH of 4.0. While Asp96 has been proposed to donate a proton to N7 under physiological conditions, at pH 4.0 it would be protonated and preclude the formation of an H-bond at the transition state. At pH 4.0 protonation might be more likely on N1 and N3 of the adenine, since Glu177 would also be protonated at this pH, thus disrupting that ion pair with Arg180 and leaving it free to protonate N3. This interpretation contrasts with the previous kinetic isotope effects (measured at pH 4.0) that were interpreted as N7 protonation. Heavy atom isotope effects at N1 and N3 might provide further insight. Multiple protonation is also the mechanism for the acid-catalyzed solvolysis of adenine nucleosides and nucleotides (*28*, *29*).

A common observation for all of the 1-azasugar compounds is that none of these gain as much in affinity over the substrate [$\Delta\Delta G = -RT \ln(K_i/K_m)$], as expected for accurate chemical mimics of the transition state (*30*). An analysis of the partitioning of ground state and transition state binding energies toward TS stabilization is of interest (*31*, *32*). One significant structural difference between all-RNA stem−loop substrates and the methylene-bridged second-generation inhibitors of Figure 3 is that the former are riboses with a 2′-hydroxyl group on the sugar while the inhibitors are deoxygenated at the equivalent position. *In vacuo* calculations suggest that the 1-azasugar moieties of these inhibitors can adopt either of the energetically similar 3′-exo and 3′-endo conformations (Figure 4) without much distortion of the nucleotide backbone. If this holds true in the context of an oligonucleotide, these could readily be accommodated in the predicted transition state-like geometry. Previous KIE studies showed that riboses in the stem−loop RNA substrates form oxacarbenium ions that have a predominantly 3′-endo conformation to allow a stabilizing hyperconjugative overlap between the p orbital of C1′ and the C2′−H2′ bond. In the same work, RTA was shown to catalyze depurination of all-DNA stem−tetraloop substrates, albeit at a much slower rate. The less constrained 2′-deoxyribooxacarbenium ion structure allows a better stabilization via hyperconjugation with either the C2′−(*pro-R*)−H2′ or the C2′−(*pro-S*)−H2′ bonds, thus decreasing the energetic barrier to its formation (*33*). It was therefore thought that the 1-azasugar mimics might also adopt the oxacarbenium ion-like conformation more easily. The lack of a commensurate gain in binding affinity is therefore surprising but consistent with the slow k_{cat} for all-DNA substrates.

Orita *et al*. (*34*) showed that an RNA stem−loop 12-mer with deoxyadenosine at the depurination site (GdAGA) is hydrolyzed ∼26 times faster than the corresponding RNA stem−loop 12mer. We observed rates that were 16 times faster and also determined the K_m of this substrate to be ∼30 μM, which is 3 times weaker than that of the substrate, A12, which has a K_m of ∼9 μM. The comparison of 1-azasugar stem−tetraloop inhibitors with their all-RNA stem−tetraloop substrate counterparts disregards the differences in catalytic relevance that may arise from a 2′-hydroxyl deletion. When rates (k_{cat} for GdAGA vs GAGA) are corrected for the intrinsic reactivity of deoxyadenosine compared to its 2′-hydroxy counterpart ($k_{solution}$) under acid solvolysis, RTA binds the GAGA substrate ∼25-fold ($k_{solution}/k_{cat}$) better than the GdAGA substrate. This reflects weaker transition state interactions for the GdAGA substrate even though its hydrolytic rate appears to be faster. The ground state/transition state binding energy paradox reveals that the deoxy structure is intrinsically more reactive (catalysis), yet it is the RNA structure that is preferred by the enzyme (binding and catalysis). RTA takes advantage of the interactions with the 2′-hydroxyl for both recognition and catalytic rate enhancement by stabilizing the oxacarbenium ion via some interaction like H-bonding with a neighboring invariant carboxylate such as Glu177. Strengthening of interactions in the transition state might be the more likely mechanism of reducing barrier heights for the reaction than ground state destabilization. The lack of crystal structures with bound oligonucleotides precludes a clear explanation.

On the basis of these observations, we can say that the current inhibitors might lack sufficient electrostatic complementarity to mimic an activated leaving group, and therefore, an approach is needed that (a) takes into account multiple protonation of the adenine and (b) does not ablate the involvement of a 2′-hydroxy group in the adenosine isostere at the depurination site.

Inhibition with RNA−Stem and Hybrid−Tetraloop-Type Hairpins. Substitution of a deoxyguanosine in the 5′-site preceding the depurination site of the A12 RNA substrate (i.e., dGAGA instead of GAGA) results in a 3-fold reducton of k_{cat}, while the K_m decreased ∼7−8-fold. The reduction in k_{cat} presumably stems from the loss of a hydrogen bond (loss of ∼3 kcal/mol) between the 2′-OH of the preceding guanosine and N7 of the 3′-site guanosine that follows the adenosine. Hairpins are dynamic structures, and the substrates of RTA belong to the GNRA (where N is any nucleotide and R is any purine) family of tetraloops which are among the most thermodynamically stable loop structures (*35*). It is likely that the transition state conformation of the GNRA tetraloop involves H-bond formation between the first and third residues on the loop (*36*, *37*). Despite the k_{cat} result, we synthesized the inhibitor, BZ5dG-10 (Figure 3), to be able to correlate structure with binding and activity (catalysis). This molecule was found to inhibit RTA with a K_i of 26 nM (Table 1 and Figure 5b). Such tight inhibition by a "one-piece" stem−loop structure is unprecedented for ricin. It should be noted, however, that this inhibitor cannot be directly compared to the single deoxyguanosine substrate since the inhibitor has dG followed by the 2′-deoxypyrrolidine. The deleterious effect of a 2′-hydroxy deletion at the depurination site on k_{cat} has already been discussed. In the case of BZ5dG-10, a similar deleterious effect on transition state complementarity caused by the 2′-deoxypyrrolidine may be augmented by the deoxyguanosine substitution in the 5′-adjacent site. It is likely that the K_i value might improve if the 2′-hydroxy substitution is reintroduced at the depurination site.

BZ5dG-10 represents a dGNRA system, and this loop structure may not populate the conformation favored for binding by RTA as much as an equivalent GNRA loop would. The fact that the inhibitor still binds as tightly as it does suggests that other loop conformations can bind to the protein but may not necessarily be productively oriented. NMR studies currently being carried out to determine the structure of hybrid tetraloops and substrate specificity kinetics will further assist the design of new inhibitors.

Unlike other nucleoside hydrolases, the design of inhibitors for RTA is a macroscopic problem since its natural substrate is a large domain on the ribosomal subunit. Binding and catalysis are likely to involve cooperativity and remote assistance. The situation is further complicated by the fact that ricin is believed to fold upon its export from the endoplasmic reticulum into the cytosol of target cells to prevent its ubiquitination. Folding may be concurrent with and assisted by RNA binding (*38*).

Characterization of Short All-DNA Stem−Tetraloop Analogues. The ribonucleoside structural components of the tetraloop, including adenosine, AMP, dinucleotide AG, and tetranucleotide GAGA, have been examined as substrates of RTA and found not to be hydrolyzed even by stoichiometric quantities of the enzyme (*12*). The first base pair (C·G) in the stem contributes to the thermodynamic stability of the loop (*35*, *39*) of RNA hairpins and certain DNA types. In the case of RNA, the absence of the stem makes the loop unstructured which might explain the lack of activity of RTA on such molecules. Deoxyribonucleoside loops, however, do not require a stem for the depurination reaction. Thus, d(GAGA) and d(CGAGAG) were both shown to be substrates that were turned over at rates of ~0.1 and ~0.3 min^{-1} and had K_m values of ~80 and ~60 μM, respectively. The lack of a 2′-hydroxyl group in DNA substrates lends them more flexibility and, despite the lack of a C·G base pair in the 4mer, possibly results in productive loop conformations being attained. The C·G base pair in the stem in case of the 6mer does not provide a large advantage for binding or catalysis. The 1-azasugar structure was incorporated into the depurination site of a small DNA oligonucleotide in an attempt to improve affinity. Inhibitors PZ-4 [d(GPZGA)] and PZ-6 [d(CGPZGAG)] containing 8-aza-9-deazaadenine moieties were synthesized, and their K_i values were found to be 28 and 32 μM, respectively (Table 1).

Inhibition by 1-Azasugars Alone and in Combination with Deazaadenines. The binding of the compound DADMe-A to RTA was also explored. This molecule had a K_i of ~85 μM (Figure 5c), a promising result relative to the values of the other small purine-like molecules that were bound less tightly. Adenosine binds more weakly than 5 mM, and formycin monophosphate (FMP) has a K_i of ~1 mM. The azasugar thus reflects some of the features of the transition state but lacks the loop structure, the phosphate backbone, and the stem.

We also explored the binding of the azasugar, DADMe-A, in the presence of 9-deazaadenine. Tanaka *et al*. demonstrated that 1N-14 and 9-deazaadenine formed a ternary complex with RTA, and this resulted in an increase in the inhibition constant (from 480 to 100 nM). It was assumed that 9-deazaadenine occupied the leaving group pocket on the enzyme (*4*). Since DADMe-A already has a 9-deazaadenyl substituent, extraneous 9-deazaadenine was not expected to improve binding. However, we determined a K_i of 20 μM for the ternary complex (Figure 5e,f) which suggests that 9-deazaadenine binds to a second site. 9-Deazaadenine alone binds to RTA with a K_d of 360 μM, but this constant is reduced to 58 μM in the ternary complex. It is known that adenine up to 2 mM activates RTA but at greater concentrations causes inhibition, suggesting the involvement of two binding sites (*40*). We suggest that the site responsible for activation might be distinct from the leaving group pocket and might also be a site that recognizes the second adenosine (GAGA) on the tetraloop substrates. Cooperativity from this site might provide a catalytically active conformation and explain the tighter binding of ternary complexes. The inhibition constant for 9-deazaadenine binding in the ternary complex with DADMe-A and RTA (58 μM) may reflect a binding to the activation site.

DADMe-A alone also activated RTA at concentrations up to 250 μM (Figure 5d) but caused inhibition at increasing concentrations in a competitive assay with A-10 as the substrate. Three different concentrations of A-10 were used in the assay (3.5, 7, and 14 μM). At low substrate concentrations, the azasugar activates more than at high A-10 concentrations, consistent with a competitive inhibition involving binding at two sites.

Characterization of a Slow Substrate of the RTA Reaction. An RNA stem−loop 12mer, A12_5dG_8dA, with deoxynucleosides at the first and last sites on the tetraloop (dGAGdA) has a k_{cat} of ~0.7 min^{-1}. We determined K_i values of 0.77 and 0.87 μM against two competitive substrates, A-10 (k_{cat} ~ 4 min^{-1}) and 6dA-12 (k_{cat} = 1600 ± 300 min^{-1}), respectively. This molecule is the highest-affinity stem−loop substrate for RTA, and these data are useful for inhibitor design. A ternary complex of this slow substrate with RTA and 9-deazaadenine improved K_i by ~4-fold to ~0.2 μM. This suggests that 9-deazaadenine in this complex probably does not bind to the leaving group site since that pocket would be filled by the 9-deazaadenine moiety of the inhibitor. The observation that binding of the stem−loop structures improves by addition of small ligands is encouraging. Such compounds might provide an increased affinity in ternary complexes of methylene-bridged inhibitors with RTA.

Binding of Methylated Adenines to RTA. The binding of adenine alone in the hypothetical active site of ricin is known from X-ray crystallographic studies. Adenine binds in a specificity pocket between the side chains of Tyr80 and Tyr123 and forms hydrogen bonds between N1 and Val81, and between the exocyclic 6-amino group and Gly121. As a result, the side chain of Tyr80 is rotated by ~45° to allow stacking. Arg180 appears to act as an acid to protonate the base on N3. As the transition state is approached, geometry optimization within the active site leads to favorable π-stacking interactions and tighter H-bonds with the appropriate residues on the enzyme.

Recently, the mechanisms by which DNA repair glycosylases distinguish neutral adenine and cationic alkylpurine bases have been elucidated, the solution structure of 3-methyladenine DNA glycosylase I in complex with its 3-methyladenine (3-MeA) cognate base has been determined, and the role of hydrogen bonding and π-cation interactions with the alkylated base has been delineated (*41*−*43*). Such mechanisms may be similarly relevant to RTA hydrolysis since

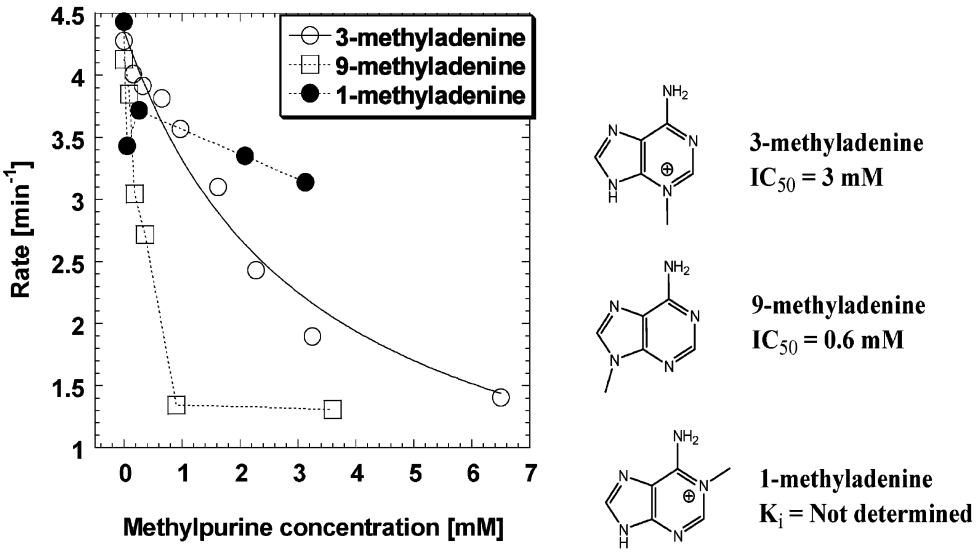

FIGURE 6: Binding of methylated adenines to RTA. The K_i for 3-methyladenine was obtained by fitting to the equation for competitive inhibition. The IC_{50} for 9-methyladenine was determined from the inhibition data.

the major catalytic force that drives this reaction is thought to be leaving group activation. Unlike the 3-methyladenine DNA glycosylase, however, the adenine of stem−loop RNA must be neutral when bound in the ground state, and as the glycosyl bond is broken at the transition state, the developing anion would induce an elevation of pK_a at either N7, N3, or N1 of the adenine. The pH profile of the RTA-catalyzed hydrolysis of A-10 is bell-shaped with maximal activity at pH ~4 (*12*). The k_{cat}/K_m decreases at increasing pH and is consistent with protonation of two groups with pK_a values of ~4. Comparison of the k_{cat}/K_m value for the hydrolysis of ribosomes with that of A-10 at pH 7.4 suggests a loss of 10^7-fold in rate enhancement. Protonation mechanisms operating at physiological pH must thus be different from those at pH ~4 in *in vitro* assays.

N3 protonation as a likely mechanism has not been investigated in detail. The pK_a of this group is <2, and it is likely that as the electrons flow into the adenine ring on glycosidic bond scission, the pK_a is elevated to near 6−7. None of the DNA glycosylases reported so far have implicated N3 protonation in catalysis, and RTA might be unique in this regard. The role of N3 protonation of adenine via such a pK_a change is reminiscent of the proposed role of N3 as a general base during peptide bond formation by domain V of 23S rRNA (*44*−*47*).

On the basis of these hypotheses, the binding of 1-methyladenine and 3-methyladenine to RTA was explored. Methylation of N1 increases its pK_a from 3.8 to 6.1 and similarly that of N3 from <2 to 6.3 (*48*). If N1 protonation and N3 protonation are the routes followed by the enzyme, then 1- and 3-methyladenines would provide a better match to the leaving group pK_a at the transition state and might be better than adenine in ternary complexes with stem−loop inhibitors and RTA. The role of N7 had already been explored using 9-deazaadenine (*4*). Methylation of N9 does not alter its pK_a significantly, but we also decided to test 9-methyladenine. The binding of all three compounds was tested using the same competitive assay that was used to characterize the stem−tetraloop inhibitors.

The *N*-methyladenines bind poorly to the enzyme (Table 1 and Figure 6) at pH 4.0. Thus, 1-methyladenine did not bind up to 3 mM; the dissociation constant for 3-methyladenine was 0.93 mM, and although 9-methyladenine was bound more tightly than its regioisomeric counterparts, its data could not be fitted to the equation for competitive inhibition. The IC_{50} for 3-methyladenine was calculated assuming competitive behavior [$K_i(1 + [S]/K_m)$] to be ~3 mM, while that for 1-methyladenine was ~0.6 mM based on the inhibition data. All three compounds are cationic at the pH of the assay. The weak binding suggests that these compounds experience either electrostatic repulsion in the active site or that their methyl groups are not sterically accommodated. The methyl group on N1 of 1-methyladenine probably precludes H-bond formation with an adverse effect on binding. The methyl group in 3-methyladenine is in the proximity of the positively charged Arg180 in the active site. The relatively better binding of 9-methyladenine is expected since the 9-methyl group can be sterically accommodated within the active site and is smaller than the sugar ring in adenosine. We determined the pK_a of N9 to be 9.5 using [8-^{13}C;9-^{15}N]adenine by two-dimensional ^{1}H−^{15}N HMBC NMR methods. At the transition state of the reaction, however, it is likely that the pK_a of N9 is reduced as the electrons that flow in begin to delocalize into N7, N1, and N3. We had taken this into consideration in our inhibitor design by employing a carbon atom instead of a nitrogen in the 9-deaza compounds. None of the methylated compounds exhibited the activation/inhibition-type kinetic pattern observed for adenine, suggesting that these may not bind to the second activation site. The data suggest that N1 may be the dominant site for protonation and that RTA may recognize neutral adenine in the ground state. Structural studies are currently being carried out in an attempt to understand these binding observations.

SUMMARY AND CONCLUSIONS

Transition state structures established from KIE studies provide crucial information about molecular events on the enzyme that are responsible for reducing reaction barrier heights and producing rates that are many orders of magnitude larger than that of the noncatalyzed reaction in solution. This information has been applied to synthesize

second-generation pyrrolidines as analogues of the transition state for RTA. Tight binding of these molecules to RTA as reported in this work has not been previously demonstrated. The precise enzymatic contacts responsible for catalysis are yet to be revealed, but our inhibition studies and the binding of the *N*-methyladenines to RTA suggest that activation of the leaving adenine moiety may occur by mechanisms that are a departure from the major involvement of N7 protonation usually seen for hydrolysis and phosphorolysis of nucleosides by most purine glycosylases. The results suggest that the design of RTA inhibitors should seek structures where the pK_a values of atoms in positions analogous to N1 and N3 are elevated. NMR and kinetic isotope studies with heavy atoms at these positions may be useful in establishing ionization states. We have also shown that a 2′-hydroxy deletion at the depurination site even in an inhibitor context is deleterious to transition state binding. We have also departed from the all-RNA stem and tetraloop inhibitors and in this study have shown that a 2′-deoxy substitution at the 5′-adjacent side of the depurination site can improve binding severalfold.

ACKNOWLEDGMENT

We thank Dr. Haiteng Deng at the Laboratory for Macromolecular Analysis and Proteomics at the Albert Einstein College of Medicine for mass spectrometry analysis.

REFERENCES

1. Endo, Y., Chan, Y. L., Lin, A., Tsurugi, K., and Wool, I. G. (1988) The cytotoxins α-sarcin and ricin retain their specificity when tested on a synthetic oligoribonucleotide (35-mer) that mimics a region of 28 S ribosomal ribonucleic acid, *J. Biol. Chem. 263*, 7917−7920.
2. Chen, X. Y., Berti, P. J., and Schramm, V. L. (2000) Ricin A-Chain: Kinetic Isotope Effects and Transition State Structure with Stem-Loop RNA, *J. Am. Chem. Soc. 122*, 1609−1617.
3. Guthrie, R. D., and Jencks, W. P. (1989) IUPAC recommendations for the representation of reaction mechanisms, *Acc. Chem. Res. 22*, 343−349.
4. Tanaka, K. S., Chen, X. Y., Ichikawa, Y., Tyler, P. C., Furneaux, R. H., and Schramm, V. L. (2001) Ricin A-chain inhibitors resembling the oxacarbenium ion transition state, *Biochemistry 40*, 6845−6851.
5. Kati, W. M., Acheson, S. A., and Wolfenden, R. (1992) A transition state in pieces: major contributions of entropic effects to ligand binding by adenosine deaminase, *Biochemistry 31*, 7356−7366.
6. Zhou, G. C., and Schramm, V. L. (2003) unpublished results.
7. Wu, M., Tang, S. L., Zang, R. J., and Yu, H. (1990) Selective killing of tumor cells in vitro by an immunotoxin composed of ricin and monoclonal antibody against Ia antigen, *Int. J. Immunopharmacol. 12*, 235−239.
8. Evans, G. B., Furneaux, R. H., Lewandowicz, A., Schramm, V. L., and Tyler, P. C. (2003) Synthesis of second-generation transition state analogues of human purine nucleoside phosphorylase, *J. Med. Chem. 46*, 5271−5276.
9. Evans, G. B., Furneaux, R. H., Tyler, P. C., and Schramm, V. L. (2003) Synthesis of a transition state analogue inhibitor of purine nucleoside phosphorylase via the Mannich reaction, *Org. Lett. 5*, 3639−3640.
10. Wu, T., Ogilvie, K. K., and Pon, R. T. (1989) Prevention of chain cleavage in the chemical synthesis of 2′-silylated oligoribonucleotides, *Nucleic Acids Res. 17*, 3501−3517.
11. Westman, E., and Stromberg, R. (1994) Removal of *tert*-butyldimethylsilyl protection in RNA-synthesis. Triethylamine trihydrofluoride (TEA, 3HF) is a more reliable alternative to tetrabutylammonium fluoride (TBAF), *Nucleic Acids Res. 22*, 2430−2431.
12. Chen, X. Y., Link, T. M., and Schramm, V. L. (1998) Ricin A-chain: kinetics, mechanism, and RNA stem-loop inhibitors, *Biochemistry 37*, 11605−11613.
13. Segel, I. (1993) *Enzyme Kinetics*, Wiley Classics Library Edition, John Wiley & Sons, New York.
14. Marcel, V., Palacios, L. G., Pertuy, C., Masson, P., and Fournier, D. (1998) Two invertebrate acetylcholinesterases show activation followed by inhibition with substrate concentration, *Biochem. J. 329* (Part 2), 329−334.
15. Luyten, I., Thibaudeau, C., and Chattopadhyaya, J. (1997) The determination of the ionization constants of C-nucleosides, *Tetrahedron 53*, 6903−6906.
16. Jiang, Y. L., Ichikawa, Y., and Stivers, J. T. (2002) Inhibition of uracil DNA glycosylase by an oxacarbenium ion mimic, *Biochemistry 41*, 7116−7124.
17. Monzingo, A. F., and Robertus, J. D. (1992) X-ray analysis of substrate analogs in the ricin A-chain active site, *J. Mol. Biol. 227*, 1136−1145.
18. Lau, A. Y., Wyatt, M. D., Glassner, B. J., Samson, L. D., and Ellenberger, T. (2000) Molecular basis for discriminating between normal and damaged bases by the human alkyladenine glycosylase, AAG, *Proc. Natl. Acad. Sci. U.S.A. 97*, 13573−13578.
19. van Oijen, A. M., Blainey, P. C., Crampton, D. J., Richardson, C. C., Ellenberger, T., and Xie, X. S. (2003) Single-molecule kinetics of lambda exonuclease reveal base dependence and dynamic disorder, *Science 301*, 1235−1238.
20. Dong, J., Drohat, A. C., Stivers, J. T., Pankiewicz, K. W., and Carey, P. R. (2000) Raman spectroscopy of uracil DNA glycosylase-DNA complexes: insights into DNA damage recognition and catalysis, *Biochemistry 39*, 13241−13250.
21. Yan, X., Hollis, T., Svinth, M., Day, P., Monzingo, A. F., Milne, G. W., and Robertus, J. D. (1997) Structure-based identification of a ricin inhibitor, *J. Mol. Biol. 266*, 1043−1049.
22. Yang, X., Gerczei, T., Glover, L. T., and Correll, C. C. (2001) Crystal structures of restrictocin-inhibitor complexes with implications for RNA recognition and base flipping, *Nat. Struct. Biol. 8*, 968−973.
23. Correll, C. C., Yang, X., Gerczei, T., Beneken, J., and Plantinga, M. J. (2004) RNA recognition and base flipping by the toxin sarcin, *J. Synchrotron Radiat. 11*, 93−96.
24. Correll, C. C., and Swinger, K. (2003) Common and distinctive features of GNRA tetraloops based on a GUAA tetraloop structure at 1.4 Å resolution, *RNA 9*, 355−363.
25. Seggerson, K., and Moore, P. B. (1998) Structure and stability of variants of the sarcin-ricin loop of 28S rRNA: NMR studies of the prokaryotic SRL and a functional mutant, *RNA 4*, 1203−1215.
26. Szewczak, A. A., and Moore, P. B. (1995) The sarcin/ricin loop, a modular RNA, *J. Mol. Biol. 247*, 81−98.
27. Day, P. J., Ernst, S. R., Frankel, A. E., Monzingo, A. F., Pascal, J. M., Molina-Svinth, M. C., and Robertus, J. D. (1996) Structure and activity of an active site substitution of ricin A chain, *Biochemistry 35*, 11098−11103.
28. Garrett, E. R., and Mehta, P. J. (1972) Solvolysis of adenine nucleosides. I. Effects of sugars and adenine substituents on acid solvolyses, *J. Am. Chem. Soc. 94*, 8532−8541.
29. Garrett, E. R., and Mehta, P. J. (1972) Solvolysis of adenine nucleosides. II. Effects of sugars and adenine substituents on alkaline solvolyses, *J. Am. Chem. Soc. 94*, 8542−8547.
30. Wolfenden, R. (2003) Thermodynamic and extrathermodynamic requirements of enzyme catalysis, *Biophys. Chem. 105*, 559−572.
31. Menger, F. M. (1992) Analysis of ground-state and transition-state effects in enzyme catalysis, *Biochemistry 31*, 5368−5373.
32. Fierke, C. A., Kuchta, R. D., Johnson, K. A., and Benkovic, S. J. (1987) Implications for enzymic catalysis from free-energy reaction coordinate profiles, *Cold Spring Harbor Symp. Quant. Biol. 52*, 631−638.
33. Chen, X. Y., Berti, P. J., and Schramm, V. L. (2000) Transition state analysis of depurination of DNA by ricin A-chain, *J. Am. Chem. Soc. 122*, 6527−6534.
34. Orita, M., Nishikawa, F., Kohno, T., Senda, T., Mitsui, Y., Yaeta, E., Kazunari, T., and Nishikawa, S. (1996) High-resolution NMR study of a GdAGA tetranucleotide loop that is an improved substrate for ricin, a cytotoxic plant protein, *Nucleic Acids Res. 24*, 611−618.
35. Heus, H. A., and Pardi, A. (1991) Structural features that give rise to the unusual stability of RNA hairpins containing GNRA loops, *Science 253*, 191−194.
36. Jucker, F. M., and Pardi, A. (1995) GNRA tetraloops make a U-turn, *RNA 1*, 219−222.

37. Jucker, F. M., Heus, H. A., Yip, P. F., Moors, E. H., and Pardi, A. (1996) A network of heterogeneous hydrogen bonds in GNRA tetraloops, *J. Mol. Biol. 264*, 968−980.
38. Lord, J. M., Deeks, E., Marsden, C. J., Moore, K., Pateman, C., Smith, D. C., Spooner, R. A., Watson, P., and Roberts, L. M. (2003) Retrograde transport of toxins across the endoplasmic reticulum membrane, *Biochem. Soc. Trans. 31*, 1260−1262.
39. Moody, E. M., and Bevilacqua, P. C. (2003) Thermodynamic coupling of the loop and stem in unusually stable DNA hairpins closed by CG base pairs, *J. Am. Chem. Soc. 125*, 2032−2033.
40. Watanabe, K., Honjo, E., Tsukamoto, T., and Funatsu, G. (1992) Fluorescence studies on the interaction of adenine with ricin A-chain, *FEBS Lett. 304*, 249−251.
41. Drohat, A. C., Kwon, K., Krosky, D. J., and Stivers, J. T. (2002) 3-Methyladenine DNA glycosylase I is an unexpected helix-hairpin-helix superfamily member, *Nat. Struct. Biol. 9*, 659−664.
42. Jiang, Y. L., Ichikawa, Y., Song, F., and Stivers, J. T. (2003) Powering DNA repair through substrate electrostatic interactions, *Biochemistry 42*, 1922−1929.
43. Cao, C., Kwon, K., Jiang, Y. L., Drohat, A. C., and Stivers, J. T. (2003) Solution structure and base perturbation studies reveal a novel mode of alkylated base recognition by 3-methyladenine DNA glycosylase I, *J. Biol. Chem. 278*, 48012−48020.
44. Nissen, P., Hansen, J., Ban, N., Moore, P. B., and Steitz, T. A. (2000) The structural basis of ribosome activity in peptide bond synthesis, *Science 289*, 920−930.
45. Ban, N., Nissen, P., Hansen, J., Moore, P. B., and Steitz, T. A. (2000) The complete atomic structure of the large ribosomal subunit at 2.4 Å resolution, *Science 289*, 905−920.
46. Moore, P. B., and Steitz, T. A. (2003) After the ribosome structures: how does peptidyl transferase work? *RNA 9*, 155−159.
47. Steitz, T. A., and Moore, P. B. (2003) RNA, the first macromolecular catalyst: the ribosome is a ribozyme, *Trends Biochem. Sci. 28*, 411−418.
48. Fuji, T., and Itaya, T. (1999) Systematic tables of mono and poly-*N*-methylated adenines: Acid dissociation constants and UV and NMR spectral data, *Heterocycles 51*, 2255−2277.

BI0498499